Nanoscale

Dynamic Article Links

Cite this: *Nanoscale*, 2012, **4**, 1620

www.rsc.org/nanoscale

PAPER

Retrieving the spatial distribution of cavity modes in dielectric resonators by near-field imaging and electrodynamics simulations

Alejandro R. Goñi,*[a] Frank Güell,[b] Luis A. Pérez,[c] Julian López-Vidrier,[d] J. Oriol Ossó,[e] Eduardo A. Coronado*[f] and Joan R. Morante[gh]

Received 9th November 2011, Accepted 16th December 2011
DOI: 10.1039/c2nr11693f

For good performance of photonic devices whose working principle is based on the enhancement of electromagnetic fields obtained by confining light into dielectric resonators with dimensions in the nanometre length scale, a detailed knowledge of the optical mode structure becomes essential. However, this information is usually lacking and can only be indirectly obtained by conventional spectroscopic techniques. Here we unraveled the influence of wire size, incident wavelength, degree of polarization and the presence of a substrate on the optical near fields generated by cavity modes of individual hexagonal ZnO nanowires by combining scanning near-field optical microscopy (SNOM) with electrodynamics calculations within the discrete dipole approximation (DDA). The near-field patterns obtained with very high spatial resolution, better than 50 nm, exhibit striking size and spatial-dispersion effects, which are well accounted for within DDA, using a wavevector-dependent dipolar interaction and considering the dielectric anisotropy of ZnO. Our results show that both SNOM and DDA simulations are powerful tools for the design of optoelectronic devices able to manipulate light at the nanoscale.

1 Introduction

The quest for further miniaturization of optoelectronic components increasingly poses the challenge of confining light effectively into nanometre scale resonators.[1] Semiconductor nanowires (NWs) are among the most promising nanostructures for that purpose, since they can be readily grown with high quality and great up-scalability, for example, by the metal-catalyst assisted vapor-liquid-solid (VLS) method.[2] By this technique, growth proceeds self-organized, resulting in wires with diameters from several tens to hundreds of nanometres and many microns in length. In this respect, ZnO and other wide-gap semiconductors are particularly suitable materials for optical resonators since they are transparent in almost the entire visible spectrum and they usually lead to very regular hexagonal-shaped, single-crystalline nanowires. Such optical cavities sustain different Fabry-Pérot (FP) modes, propagating along the wire axis or bouncing between two opposing hexagonal facets. In addition, whispering gallery modes (WGM) are expected to be dominant in such nanoresonators due to the low losses and high Q-factors they exhibit.[3] ZnO presents as added value a huge exciton binding energy of about 60 meV, responsible for the clear observation of polaritonic effects at room temperature.[4]

A variety of optoelectronic nanodevices and nanophotonic systems contain NW resonators as an active part, ranging from light emitting cavities,[3,6–10] lasers,[5,11–13] frequency converters,[14] sensors,[15,16] solar cells,[17] and waveguide devices.[18–23] The performance of these devices depends much on the mode structure, *i.e.*, the spatial distribution of the electromagnetic field of the active cavity mode. Thus, a detailed knowledge of the mode structure is essential for a rational design of any device or for the fundamental understanding of its working principle. From the experimental point of view, though, this fundamental knowledge is still lacking. Most of the high-resolution optical studies reported so far deal with the spectral dependence of the emission and the waveguiding properties of NWs made of wide-gap materials observed in the *far field*, having a spatial resolution limited by the wavelength of the light.[8,9,11,18,21–23] On the contrary, much less is known about the near-field distribution. In the

[a]*ICREA & Institut de Ciència de Materials de Barcelona (ICMAB-CSIC), Esfera UAB, E-08193, Bellaterra, Spain. E-mail: goni@icmab.es*
[b]*Departament d'Electrònica, Universitat de Barcelona, E-08028, Barcelona, Spain*
[c]*INFIQC, CLCM, Departamento de Fisicoquímica, Facultad de Ciencias Químicas, Universidad Nacional de Córdoba, Córdoba, 5000, Argentina*
[d]*Departament d'Electrònica, Universitat de Barcelona, E-08028, Barcelona, Spain*
[e]*MATGAS Research Center, Campus de la UAB, E-08193, Bellaterra, Spain*
[f]*INFIQC, CLCM, Departamento de Fisicoquímica, Facultad de Ciencias Químicas, Universidad Nacional de Córdoba, Córdoba, 5000, Argentina. E-mail: coronado@fcq.unc.edu.ar*
[g]*IREC-Institut de Recerca de l'Energia de Catalunya, E-08019, Barcelona, Spain*
[h]*Departament d'Electrònica, Universitat de Barcelona, E-08028, Barcelona, Spain*

pioneering work of Johnson *et al.*,[5] it was possible to assess by SNOM measurements if the near-bandgap emission in the ultraviolet (UV) was stemming from the ZnO wire ends or from the upper side along the entire wire, depending upon the excitation being above or below the lasing threshold, respectively. In contrast, our previous work on ZnO NWs is concerned with the detection of the near field generated by radiative recombination processes related to defects with characteristic energies in the visible part of the spectrum (the so-called green–yellow–orange luminescence bands).[24,25] We were able to obtain direct images of the associated near fields with a spatial resolution better than 100 nm, but the low contrast made a mode assignment practically impossible.[25]

From the theoretical point of view the situation is more satisfactory, as far as the calculation of near-field intensity patterns is concerned. On the one hand, several fully-vectorial finite-element calculations of the waveguiding properties of hexagonal nanowires were undertaken to determine the electromagnetic field distribution of Fabry-Pérot modes in ZnO NWs with different purposes. They were used for example to compute the reflectivity for lowest-order guided FP modes, estimating optical gain thresholds and quality factors,[26] and to model evanescent fields for ZnO nanorod optical sensors.[15] Finite-element methods were also applied to study polarization and mode structure of the luminescence and lasing from single ZnO NWs at energies near the fundamental band gap, taking into account the exciton–polariton dispersion relations.[13] On the other hand, the boundary element method (BEM) seems very suitable for calculations of resonance frequencies, lifetimes, and near-field as well as far-field patterns of the so-called whispering gallery modes in resonators with axial symmetry such as nanowires.[3,19,27] In this case, the theoretical analysis of the WGMs reduces to the two-dimensional problem of resonant modes in dielectric resonators of regular hexagonal geometry. All these methods, although extremely successful at simulating the mode structure for radiation due to spontaneous and/or stimulated emission, seem to be much less effective at the description of the electromagnetic field distribution under conditions of constant illumination. This situation is often encountered in SNOM experiments as well as for the measurement of the reflectivity or extinction coefficient, which depend much on the nature, polarization, direction and energy of the incident wave. In this respect, the discrete dipole approximation appears as the best candidate to tackle such electrodynamics problems. It results somewhat astonishing that despite the overall success of DDA in the field of plasmonics, where it has been employed to calculate plasmon resonances and their associated near and far-field patterns in all kinds of metallic nanostructures,[28–32] its application to dielectric resonators is practically absent.

In this work, we demonstrate that by combining SNOM and electrodynamics simulations within DDA we are able to attain deeper understanding of the phenomena that determine the optical mode structure at the nanoscale in hexagonal dielectric resonators consisting in individual ZnO nanowires. We show that spatial dispersion effects which are taken into account theoretically by using a wavevector dependent dipolar interaction are significantly influencing the electromagnetic field distribution inside and outside the NW already for diameters larger than 50 nm. Furthermore, we find out that the near-field pattern of individual nanowires strongly depends on wire size, the wavelength of the incident light and its linear polarization (parallel or perpendicular to the NW axis). These effects are more pronounced for photon energies that roughly match those of the different excitonic transitions near the absorption edge of ZnO, mainly due to the strong tensorial character and marked anisotropy of the complex dielectric function at those frequencies. These findings provide basic information for the rational design of optoelectronic devices in which the manipulation of light at the nanoscale is a key feature.

2 Results and discussion

Fig. 1 summarizes the SNOM results obtained in transmission–collection mode for two representative wires. Fig. 1(a) and (d) show the topographic images of a wire piece measured in an area of roughly 2 × 2 μm. The indicated diameters were inferred directly from the vertical displacement of the SNOM tip along a corresponding line scan across the wire (see Fig. 2). In contrast, the apparent lateral dimensions are not representative for the actual wire size due to tip-convolution effects. A closer inspection of the topographic images indicates that the NWs are always lying on the substrate supported by one hexagonal facet. Fig. 1(b) and (c) and 1(e) and (f) display the SNOM images of the two wires obtained by exciting with two different laser wavelengths; one in the UV with an energy very close to that of the fundamental gap of ZnO and the other in the visible, where the material is transparent. We point out that for each wire the SNOM images for different colors were collected in successive scans without retracting the tip from its feedback position, which allowed us to map out exactly the same region. The feature richness and the high contrast of all SNOM images, which are totally reproducible even for measurements performed on different days and with different probes, are striking. Mainly for UV illumination at 378 nm we observe a clear pattern of extremely sharp lines that depends much on wire size. For a variation in wire diameter only from 220 to 270 nm the SNOM pattern changes from one with two bright lines going roughly along the edges of the top facet of the smaller wire to a pattern with a series of approximately parallel lines, in which the most intense one appears at the top-facet center of the larger wire [see Fig. 1(b) and (e)]. The SNOM images radically change again for visible illumination, as observed in the (c) and (f) panels of Fig. 1 for red excitation at 633 nm. Similar results were obtained for blue, green and near IR illumination. Thus, in the transparent region, the near-field spatial distribution appears to be weakly influenced by size effects: patterns exhibit a broad and intense band running all along the top facet of the wire. The only apparent dependence of the SNOM pattern on laser wavelength consists of an increase in the period of the intensity modulation along the wire axis of the broad band at the top facet center, according to the increase in wavelength of the light used for illumination.

For further analysis of the SNOM results and to compare them with the DDA simulations it is instructive to study in detail topographic line profiles across the wire, as exemplified in Fig. 2. Taking into account tip convolution effects, valuable information about the wire as well as the SNOM tip is obtained. The diameter D, as defined in the figure, is directly given by the

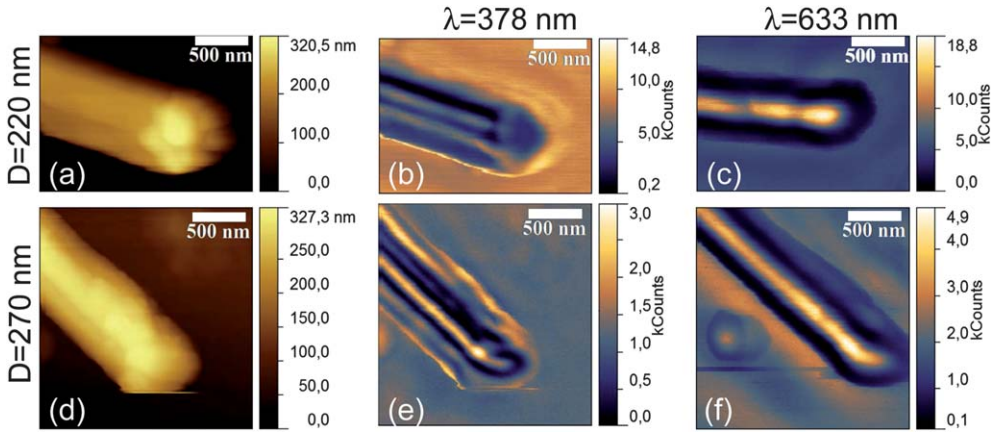

Fig. 1 (a) and (d) Topography images of a single ZnO NW with a diameter of 220 and 270 nm, respectively, lying on a sapphire substrate as measured online using the SNOM tip. (b)–(c) and (e)–(f) Corresponding SNOM images obtained in transmission–collection mode for excitation in the UV at 378 nm and with red laser light at 633 nm, as indicated.

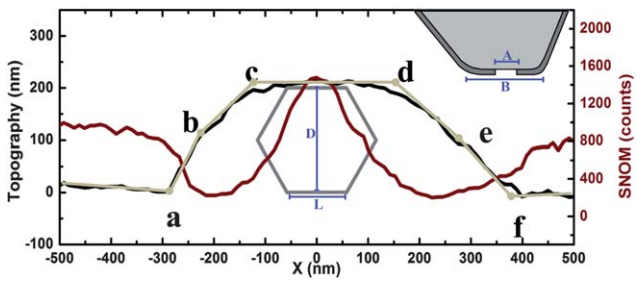

Fig. 2 Representative topography and SNOM line-scan profiles across a ZnO NW. The curve constructed piecewise with the segments a–b–c–d–e–f out of the topographic trace is used for a realistic reconstruction of the scanned wire and the SNOM tip; the former represented by the hexagon and the latter as sketched in the inset. D and L are the wire diameter and facet length, respectively, whereas B and A represent the size of the tip apex and its aperture, respectively.

topographic height of the wire. The $\overline{cd}$ segment in Fig. 2 is roughly determined by the upper flat part of the topographic profile, corresponding to the movement of the SNOM tip as it flies at constant distance over the top facet. Its length should be equal to $L + B$, where $L = D/\sqrt{3}$ is the facet length and B is the lateral size of the tip apex. Finally, the segments $\overline{ab}$ and $\overline{ef}$ correspond to the traces of the tip described when it goes up or down keeping constant the distance from its side wall to the corresponding hexagon corner at each side of the wire. The slope of these segments corresponds to an angle between 30° to 40° from the vertical, which is very close to the apex angle of the tip. This allows us to construct the sketch of the SNOM probe shown in the inset to Fig. 2.

In order to deepen into our understanding of the experimental findings beyond a mere phenomenological description, we have performed electrodynamics simulations within the discrete dipole approximation; an accurate numerical method in which an object of arbitrary shape is represented as a cubic lattice of N polarizable points.[33,34] As described elsewhere,[28,29] we consider that the jth element at the site position $\mathbf{r}_j$ has a dipole polarizability α_j, which is obtained from the complex, frequency-dependent dielectric function $\varepsilon(\omega)$ of the material, such that the cubic array of dipoles reproduces the dielectric response of the extended object to electromagnetic radiation. For anisotropic materials like ZnO ε is a tensor. The polarization $\mathbf{P}_j$ induced by the *local* electric field $\mathbf{E}_{\mathrm{loc}}$ at the site of the jth element is written as $\mathbf{P}_j = \boldsymbol{\alpha}_j \cdot \mathbf{E}_{\mathrm{loc}}(\mathbf{r}_j)$. For an array of discrete dipoles the local field is the sum of the incident field and the contribution from all other dipoles:

$$\mathbf{E}_{\mathrm{loc}}(\mathbf{r}_j) = \mathbf{E}_0 \exp(i\mathbf{k}\cdot\mathbf{r}_j) - \sum_k \mathbf{A}_{jk}\cdot\mathbf{P}_k, \quad \mathbf{A}_{jj} = \boldsymbol{\alpha}_j^{-1}, \ j = 1, 2, ..., N, \tag{1}$$

where $\mathbf{E}_0$ and $\mathbf{k}$ are the amplitude and wavevector of the incident field, respectively. The matrix $\mathbf{A}$ which takes into account the interaction between each dipole and the rest of the array is given by:

$$\mathbf{A}_{jk}\cdot\mathbf{P}_k = \frac{\exp(i\mathbf{k}\cdot\mathbf{r}_{jk})}{r_{jk}^3}\left\{k^2\mathbf{r}_{jk}\times(\mathbf{r}_{jk}\times\mathbf{P}_k) + \frac{1 - i\mathbf{k}\cdot\mathbf{r}_{jk}}{r_{jk}^2}\left[r_{jk}^2\mathbf{P}_k - 3\mathbf{r}_{jk}(\mathbf{r}_{jk}\cdot\mathbf{P}_k)\right]\right\} \quad k \neq j, \tag{2}$$

with $\mathbf{r}_{jk} = \mathbf{r}_j - \mathbf{r}_k$. We note that the calculations account for spatial dispersion effects, including a wavevector dependent dipolar interaction as in 2. By combining 1 and 2, the numerical problem is reformulated as a set of $3N$ complex linear equations, which has to be solved to obtain the polarization vector $\mathbf{P}$ at any point in space from which the near field or other optical properties can be calculated.

The DDA simulations were performed for two different wire diameters of 220 and 295 nm and lengths of 2 and 2.5 μm, respectively. The small(large) wire was supported by a substrate of 1.6 × 2.3 μm²(2.1 × 3.0 μm²) in size consisting in a 24 nm(32 nm) thick sapphire layer and a thin top ZnO layer of 6 nm(8 nm) in thickness. In both cases, about 1×10^6 dipoles were used to describe the whole target, from which 4×10^5 dipoles were used to construct the wire and the rest for the substrate. Accordingly, the dipole spacing was 5.9 and 7.8 nm for the small and large wire, respectively. The illumination proceeded from the substrate side in form of a monochromatic

plane wave with the experimental wavelength values and linear polarization either parallel or perpendicular to the wire axis. The refractive index $n(\omega)$ and extinction coefficient $\kappa(\omega)$ of sapphire[35] and the corresponding tensor components parallel and perpendicular to the hexagonal axis of wurtzite ZnO were taken from the literature for the UV[36,37] and visible spectral range.[38]

We first discuss the DDA results concerning finite size effects, which are summarized in Fig. 3 for both wire diameters corresponding to the SNOM data[39] shown in Fig. 1 for UV excitation at 378 nm. At this wavelength the SNOM patterns exhibit a clear wire size dependence, most likely due to the fact that the incoming light is almost resonant with excitonic transitions at the fundamental gap of ZnO, leading to significant light absorption and dielectric anisotropy. Fig. 3(a) and (d) show cross sectional contour plots of the electromagnetic field enhancement distribution, depicted on a logarithmic scale. This represents the calculated ratio of the squared modulus of the complex electric-field vector at each point in space divided by the intensity of the incident light, summing up the contributions of both linear polarizations. White/red areas correspond to regions of high electromagnetic field intensity, whereas blue/black areas indicate the dark regions. The first result concerns the field distribution inside the ZnO NWs, as depicted in Fig. 3(a) and (d), which indicates that the larger wire is able to confine a higher order mode with four nodes in the vertical direction, as compared to the mode within the smaller wire, which exhibits three nodes. This appears to have a large impact on the near field sensed by the SNOM probe, as discussed below. The marked asymmetry of the enhancement contours in the direction of the incoming plane wave is due to the combined effect of spatial dispersion and finite size, for the contours become totally symmetric at wire diameters below 50 nm. We notice that the presence of the transparent substrate influences the degree of confinement of the optical mode, leading to a certain leakage of electromagnetic field intensity towards the substrate. We notice that the clear interference pattern with bright/dark regions alternating along the substrate is also experimentally observed (see Fig. 1).

For a better comparison with the experiment we have employed the simulated field distribution to compute the integrated field intensity probed by a *theoretical* tip with an aperture of 40×40 nm^2 while moving along the line profiles directly taken from the corresponding measured topography. Again we computed the field enhancement but plotted it on a linear scale. Hence, Fig. 3(b) and (e) represent the *simulated* SNOM profiles which are to be compared with the measured ones of Fig. 1(b) and (e). The qualitative agreement between calculated and measured near field distributions is remarkable. We point out that, in spite of the strong absorption experienced by light at 378 nm, the confined cavity mode produces an enhancement of the electromagnetic near-field intensity outside the wire up to a factor of two. This might have implications for applications in molecular sensors, for instance. Panels (c) and (f) of Fig. 3 show a set of typical line profiles across the wire of the topography and both measured and simulated SNOM images. We note that the simulated profiles reproduce all features of the experimental ones, although there are some discrepancies in the position of intensity maxima and minima. We believe this is due to uncertainties in the values of the refractive index and extinction coefficient taken from the literature, since the dielectric properties of nanowires at frequencies close to the gap energy might differ from that of bulk ZnO. Nevertheless, the simulations allow us to trace back the origin of the features observed in the SNOM scans of the NWs. The near field would exhibit maxima at the center or at the edges of the top facet depending on the peculiarities of the cavity mode being active, which, in turn, is determined by the wire size and the

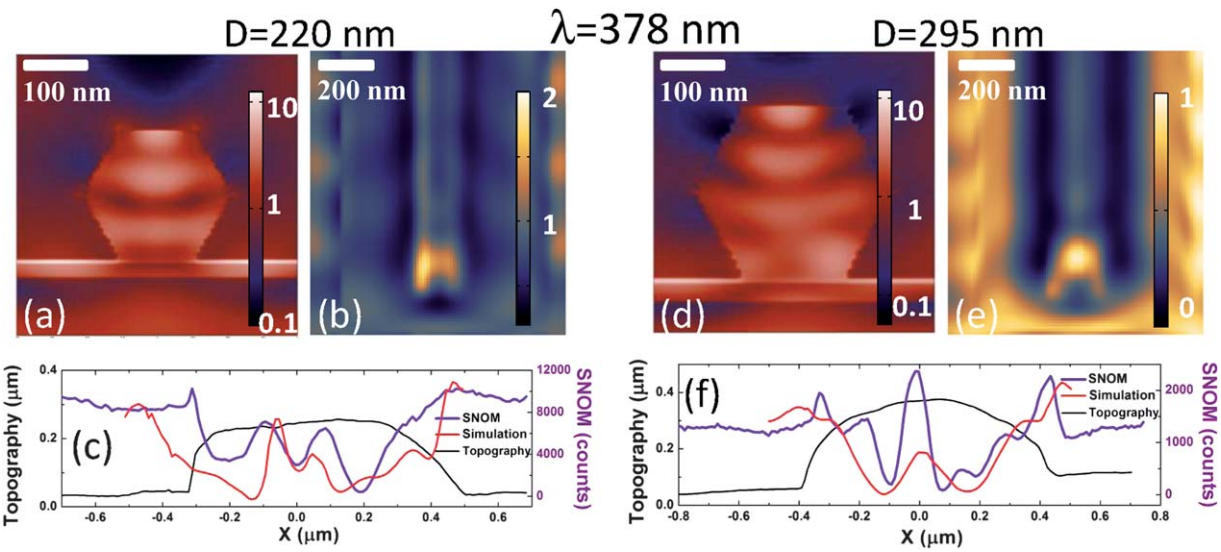

Fig. 3 (a) and (d) Cross sectional contour plots of the electromagnetic field enhancement distribution, depicted on a logarithmic scale, as calculated within DDA for a ZnO NW of 220 and 295 nm in diameter, respectively, supported by a sapphire substrate and for the case of UV excitation at 378 nm. (b) and (e) Corresponding simulated SNOM images constructed by integrating the electromagnetic field intensity calculated within DDA over the size of a theoretical aperture describing the same trace of the SNOM tip, as given by the measured topography line profiles. (c) and (f) Topography and SNOM line-scan profiles of the smaller and larger NW, respectively, together with the line profiles obtained from the corresponding *simulated* SNOM images for comparison.

wavelength of the mode. The fine structure observed mainly in the SNOM scans of the larger wire stems from the near-field enhancements generated by the cavity mode near the center of the facets at both sides of the NW; regions of high intensity which extend surprisingly far outside the wire.

Finally, we discuss the DDA results on the wavelength dependence in the transparency region. Fig. 4 shows again the cross sectional contour plots and simulated near-field images together with the SNOM and topography line profiles for the small wire in case of red and near IR illumination. The outcome of the simulations is that for all studied wavelengths in the transparency spectral region the ZnO NW essentially confines the same mode characterized by a strong lobe close to the upper hexagonal facet and a node near the basal facet. This kind of "leaky" cavity mode is certainly a consequence of the presence of the transparent substrate. Consequently, the optical near field outside the wire reaches its maximum enhancement in excess of a factor of two at the immediate vicinity of the whole top facet. As can be seen from Fig. 4(b) and (e), such near-field distribution rather than being uniform along the wire, it displays an intensity modulation, whose period nicely scales with the wavelength of the excitation. The line profiles demonstrate that in this spectral region an excellent quantitative agreement between theory and experiment is achieved. For red excitation the DDA simulated profile reproduces the observed features not only in position and linewidth but also the relative intensities of the central peak and the near field at the substrate surface are accurately calculated. The simulated profile for excitation at 785 nm, however, exhibits two sharp peaks at both sides of the broad central band, which are associated with the contribution to the near field from the incident-light component with linear polarization perpendicular to the wire axis. This might be an indication of residual polarization of the laser beam along the wire.

3 Conclusions

In summary, using SNOM we have been able to map out the near field of cavity modes confined to ZnO NWs with high spatial resolution, finding striking differences between patterns as a function of wire size, incident laser wavelength, degree of polarization, *etc.* Electrodynamics calculations of the spatial distribution of electromagnetic fields in supported hexagonal wire resonators within the discrete dipole approximation provide a key insight to understand the experimental findings. For instance, electromagnetic field enhancements in the vicinity of a nanowire are possible and its actual pattern would depend critically on size and wavelength. Polarization and direction of propagation of the incident light play also a role, as well as the degree of transparency of the substrate supporting the wire. We conclude that the excellent qualitative and, in some cases, quantitative agreement between theory and experiment mutually validates the SNOM technique and the DDA simulation method as powerful tools in nanoscience and nanotechnology. The high levels of detail attained for revealing the underlying physics of optical modes confined at the nanoscale is an essential feature for the development and design of optoelectronic devices. Finally, the applicability of these techniques is not restricted to ZnO or other dielectric materials, for their use is readily extended to any optically sensing device, for example, the ones based on plasmonic nanostructures.

4 Experimental

Single-crystal ZnO nanowires (NWs) with lengths and diameters ranging from 0.4 to 40 μm and 100 to 300 nm, respectively, were grown by the vapor–liquid–solid process introducing Au as metal catalyst. The gold was previously deposited on a sapphire

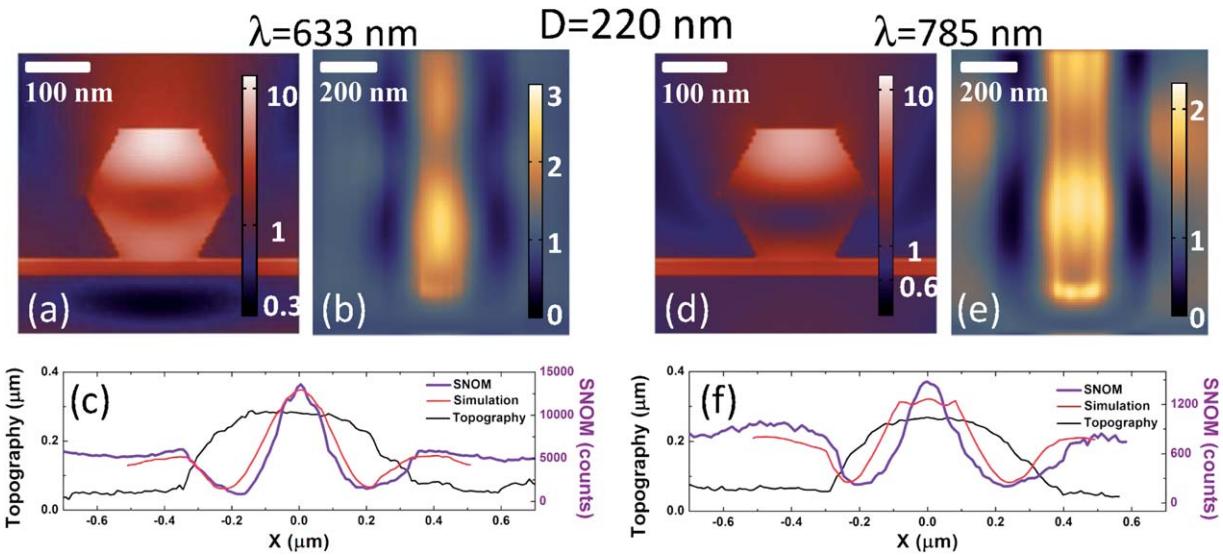

Fig. 4 (a) and (d) Cross sectional contour plots of the electromagnetic field enhancement distribution, depicted on a logarithmic scale, as calculated within DDA for a ZnO NW of 220 nm in diameter, using laser light excitation in the red (633 nm) and near IR (785 nm), respectively. (b) and (e) Corresponding simulated SNOM images constructed by integrating the electromagnetic field intensity calculated within DDA over the size of a theoretical aperture describing the same trace of the SNOM tip, as given by the measured topography line profiles. (c) and (f) Topography and SNOM line-scan profiles of the smaller NW for red and near IR illumination, respectively, together with the line profiles obtained from the corresponding *simulated* SNOM images for comparison.

substrate by sputtering thin layers. Upon heating, the Au layer will turn into high-density Au clusters and the ZnO NWs grow over the sputtered regions. The synthesis was carried out at 900 °C inside a horizontal quartz tube, using Ar as carrier gas and a mixture of ZnO and graphite powder as precursor. Structural characterization was performed by field-emission scanning electron microscopy (FESEM) and high-resolution transmission electron microscopy (HRTEM).[24,25] Fig. 5(a) shows a FESEM image of a dense ensemble of ZnO NWs, as it grows inside the squares where Au was sputtered. This image highlights the overall vertical orientation of the wires, resulting from the compatibility between the lattice parameter of ZnO and the crystalline sapphire substrate. The densely populated square regions are typically surrounded by several sparse isolated wires that might have fallen off onto the substrate during or after growth, as exemplified in Fig. 5(b). In addition, HRTEM micrographs reveal that the ZnO NWs are of high crystalline quality and grow preferentially along the [0001] direction, having hexagonal cross section.[25]

Patterns of the near-field intensity of individual ZnO NWs were recorded with a Veeco Aurora-III system equipped-with a photomultiplier detector. The SNOM probe was operated in shear-force feedback conditions with a tuning-fork working at 100 kHz and keeping constant a probe-to-sample distance of about 10 nm during scans. All measurements were performed in transmission–collection mode, in which the illumination proceeds from below and through the substrate by focusing the light with a 50× microscope objective and the near-field signal is collected by the SNOM tip. In this way, we attained sub-wavelength spatial resolution in excess of 50 nm. Five different laser wavelengths from the ultraviolet (UV) to the near infrared (IR) were available for excitation: 378, 488, 514, 633, and 785 nm. Special care was taken to depolarize the incident beam as much as possible. All optical measurements were carried out at room temperature.

Acknowledgements

This work was supported by the Spanish Ministry of Science and Innovation (MICINN) through Grants CSD2010-00044 (Consolider NANOTHERM) and CSD2009-00050 (Consolider MULTICAT) and by the CICyT National Project NANO-ENESTO (MAT2010-21510). JOO acknowledges support from the ICREA-JE program. LAP and EAC acknowledge the Argentinean CONICET, the ANPCyT and the SECyT-UNC for financial support.

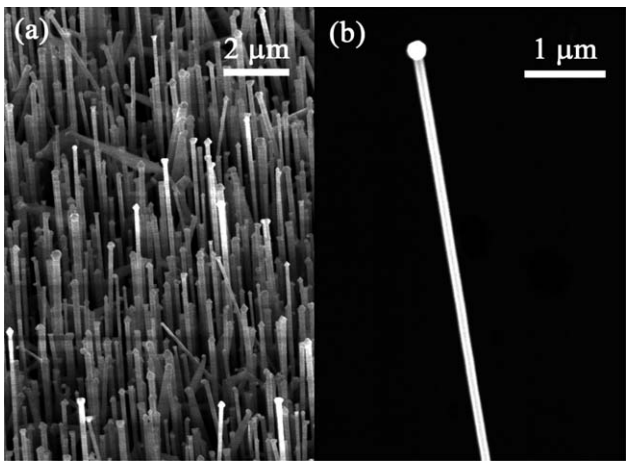

Fig. 5 (a) A field-emission SEM image of a dense ensemble of single-crystal ZnO nanowires grown on a sapphire substrate. (b) A SEM image of an isolated ZnO wire with the Au catalyst at its tip.

References

1 A. B. Djurišić and Y. H. Leung, *Small*, 2006, **2**, 944.
2 H. J. Fan, P. Werner and M. Zacharias, *Small*, 2006, **2**, 700.
3 C. Czekalla, T. Nobis, A. Rahm, B. Cao, J. Zúñiga-Pérez, C. Sturm, R. Schmidt-Grund, M. Lorenz and M. Grundmann, *Phys. Status Solidi B*, 2010, **247**, 1282, and references therein.
4 Ü Özgür, Y. I. Alivov, C. Liu, A. Teke, M. A. Reshchikov, S. Doğan, V. Avrutin, S.-J. Cho and H. Morkoç, *J. Appl. Phys.*, 2005, **98**, 041301.
5 J. C. Johnson, H. Yan, R. D. Schaller, L. H. Haber, R. J. Saykally and P. Yang, *J. Phys. Chem. B*, 2001, **105**, 11387.
6 T. Nobis, E. M. Kaidashev, A. Rahm, M. Lorenz and M. Grundmann, *Phys. Rev. Lett.*, 2004, **93**, 103903.
7 I. Shalish, H. Temkin and V. Narayanamurti, *Phys. Rev. B: Condens. Matter Mater. Phys.*, 2004, **69**, 245401.
8 L. K. Van Vugt, S. Rühle, P. Ravindran, H. C. Gerritsen, L. Kuipers and D. Vanmaekelbergh, *Phys. Rev. Lett.*, 2006, **97**, 147401.
9 S. Rühle, L. K. van Vugt, H.-Y. Li, N. A. Keizer, L. Kuipers and D. Vanmaekelbergh, *Nano Lett.*, 2008, **8**, 119.
10 L. K. Van Vugt, B. Zhang, B. Piccione, A. A. Spector and R. Agarwal, *Nano Lett.*, 2009, **9**, 1684.
11 J. C. Johnson, H. Yan, P. Yang and R. J. Saykally, *J. Phys. Chem. B*, 2003, **107**, 8816.
12 C. Czekalla, C. Sturm, R. Schmidt-Grund, B. Cao, M. Lorenz and M. Grundmann, *Appl. Phys. Lett.*, 2008, **92**, 241102.
13 H.-Y. Li, S. Rühle, R. Khedoe, A. F. Koenderink and D. Vanmaekelbergh, *Nano Lett.*, 2009, **9**, 3515.
14 J. C. Johnson, H. Yan, R. D. Schaller, P. B. Petersen, P. Yang and R. J. Saykally, *Nano Lett.*, 2002, **2**, 279.
15 S. Börner, C. E. Rüter, T. Voss, D. Kip and W. Schade, *Phys. Status Solidi A*, 2007, **204**, 3487.
16 T. Chen, G. Z. Xing, Z. Zhang, H. Y. Chen and T. Wu, *Nanotechnology*, 2008, **19**, 435711.
17 M. Law, L. E. Greene, J. C. Johnson, R. J. Saykally and P. Yang, *Nat. Mater.*, 2005, **4**, 455.
18 M. Law, D. J. Sirbuly, J. C. Johnson, J. Goldberger, R. J. Saykally and P. Yang, *Science*, 2004, **305**, 1269.
19 T. Nobis, E. M. Kaidashev, A. Rahm, M. Lorenz and M. Grundmann, *Phys. Rev. Lett.*, 2004, **93**, 103903.
20 S. K. Donthu, Z. Pan, G. S. Shekhawat, V. P. Dravid, B. Balakrisnan and S. Tripathy, *J. Appl. Phys.*, 2005, **98**, 024304.
21 T. Voss, G. T. Svacha, E. Mazur, S. Müller, C. Ronning, D. Konjhodzic and F. Marlow, *Nano Lett.*, 2007, **7**, 3675.
22 Z. Zhang, H. Yuan, Y. Gao, J. Wang, D. Liu, J. Shen, L. Liu, W. Zhou, X. Zhu, Y. Zhao and L. Sun, *Appl. Phys. Lett.*, 2007, **90**, 153116.
23 B. Piccione, L. K. van Vugt and R. Agarwal, *Nano Lett.*, 2010, **10**, 2251.
24 F. Güell, J. O. Ossó, A. R. Goñi, A. Cornet and J. R. Morante, *Superlattices Microstruct.*, 2009, **45**, 271.
25 F. Güell, J. O. Ossó, A. R. Goñi, A. Cornet and J. R. Morante, *Nanotechnology*, 2009, **20**, 315701.
26 A. V. Maslov and C. Z. Ning, *Appl. Phys. Lett.*, 2003, **83**, 1237.
27 J. Wiersig, *Phys. Rev. A: At., Mol., Opt. Phys.*, 2003, **67**, 023807.
28 K. L. Kelly, E. A. Coronado, L. L. Zhao and G. C. Schatz, *J. Phys. Chem. B*, 2003, **107**, 668.
29 R. Encina and E. A. Coronado, *J. Phys. Chem. C*, 2007, **111**, 16796.
30 M. Rang, A. C. Jones, F. Zhou, Z.-Y. Li, B. J. Wiley, Y. Xia and M. B. Raschke, *Nano Lett.*, 2008, **8**, 3357.
31 E. R. Encina, E. M. Perassi and E. A. Coronado, *J. Phys. Chem. A*, 2009, **113**, 4489.
32 E. M. Perassi, J. C. Hernández-Garrido, M. S. Moreno, E. R. Encina, E. A. Coronado and P. A. Midgley, *Nano Lett.*, 2010, **10**, 2097.
33 E. M. Purcell and C. R. Pennypacker, *Astrophys. J.*, 1973, **186**, 705.

34 B. T. Draine, *Astrophys. J.*, 1988, **333**, 848.
35 *Handbook of Optics (Volume IV)*, ed. M. Bass, McGraw-Hill, New York, 3rd edn, 2009.
36 M.-I. Kang, S. W. Kim, Y.-G. Kim and J.-W. Ryu, *J. Korean Phys. Soc.*, 2010, **57**, 389.
37 R. Schmidt-Grund, P. Kühne, C. Czekalla, D. Schumacher, C. Sturm and M. Grundmann, *Thin Solid Films*, 2011, **519**, 2777.
38 K. Postava, H. Sueki, M. Aoyama, T. Yamaguchi, Ch. Ino, Y. Igasaki and M. Horie, *J. Appl. Phys.*, 2000, **87**, 7820.
39 In the calculations, we used for the larger wire a diameter of 295 nm instead of 270 nm, for which good qualitative agreement between simulated and measured near-field distributions was attained.

